In silico modeling and virtual screening for identification of inhibitors for SWP12 and SWP30 in *Nosema bombycis*

Khushboo Tripathi[1], Eshita Kamal[1], Prashanth Karunakar[2], Shanti K.N.[1*], Karuna B.S.[1], Rhea Harish[1] and Vamsi Krishna K.[1]

1. Department of Biotechnology, PES University, Bangalore, 560085, INDIA
2. Department of Biotechnology, Dayananda Sagar College of Engineering (Affiliated to Visveswaraya Technological University, Belagavi), Bangalore, 560111, INDIA
*shantikoppala@pes.edu

Abstract

Bombyx mori, an insect, is of great economic value, widely known for the production of silk. Nosema bombycis, an intracellular parasite, often infects it and causes a fatal disease - Pebrine which affects the development of the worm. The infected larvae of the silkworms are coated with a brown spot. It also causes loss of appetite, makes them sluggish and opaque, ultimately resulting in death. The proteins studied here are SWP12 and SWP30, both of which are an exosporal protein found in N.bombycis. SWP12 is a chitin-binding protein, involved in the development of spore walls. It acts as an important surface protein of N. bombycis.

It facilitates microsporidial spore maintenance. NbSWP12 is located on the cytoskeleton as well as the spore coat of N. bombycis. The developmental stage at which it is expressed is not known.

SWP30 plays a role in sporulation, leading to the formation of a cellular spore. It is capable of binding to deproteinated chitin spore coats (DSCSs). It is expressed in the spore wall and synthesized during sporogony. This study deals with pebrine infection in Bombyx mori due to the pathogen Nosema bombycis. The infection leads to poor quality of silk production and loss of batches due to high mortality upon infection. The structure of spore wall protein present on N. bombycis was built by employing homology modelling technique. Virtual screening was conducted on a ligand library to discover lead compounds. 100ns molecular dynamics (MD) simulation was performed. RMSD, RMSF and Radius of Gyration were analyzed to determine the stability of the modeled protein and protein ligand complexes. Through virtual screening and docking studies, ligand molecules ZINC000067910920 and ZINC000035458200 were obtained as a potential drug-like molecule.

Keywords: Bombyx mori, Spore Wall Protein 12, Spore Wall Protein 30, Molecular docking, Molecular dynamics, Drug-like molecule.

Introduction

Pebrine disease affects the silkworm (*Bombyx mori*) caused by an infection from the microsporidia *Nosema bombycis*. The disease is transmitted among hosts via infected mulberry leaves or transovarially. *Nosema bombycis* infects the host organism at all the stages of development, affecting all insect tissues, with symptoms observable from the egg to the adult moth stage. *N. bombycis* maintains a close interaction with the cell cytoplasm of the host for several days, acquiring energy from the host. The symbiotic relationship between the host cell and the parasite can be sustained as *N. bombycis* averting the production of reactive oxygen species (ROS) and host cell apoptosis to create optimal environmental conditions conducive to its growth and proliferation.

The infected eggs exhibit irregular shapes, lack adherence to the substrate and hatch asynchronously. Some eggs may be dead or sterile. Larvae affected by pebrine disease typically display blackish-brown spots making them unable to produce any silk thread. They lose appetite, become sluggish, opaque and ultimately die[8]. When the microsporidia are close to the host cell and the environmental parameters are right, one of the two pathways through which they invade the cell, is the extrusion of the polar tube. In order to cause infection and to stimulate the germination of fresh spores, the polar tube injects the infectious sporoplasm into the host cell. Before the polar tube is extruded, the microsporidia are absorbed by the host cell by phagocytosis, which results in the alternate invasion pathway. The sporoplasm is released into the host cell cytoplasm when the polar tube is extruded to bypass the maturing lysosome after it has entered the cell[2] . After that, the sporoplasm germinates inside the host cell in a manner akin to the preceding one.

Most of the mortality occurs shortly after the second instar when the infection is acquired by the larvae transovarially from a mother silkworm moth. The surviving larvae, if they pass the third instar, appear small, pale and flaccid. Infected silkworm moths that reach adulthood often exhibit impaired wings and disfigured antennae. The scales on the abdomen and wings fall off easily too. Adult moths were infected by pebrine mate poorly and produce eggs of low quality[11].

For years the silk industry has faced financial challenges due, to Pebrine disease caused by the microsporidian *Nosema bombycis.* The parasite spreads widely within the

colony both horizontally and vertically leading to infection[7]. Research by He et al reveals that the parasite infiltrates host cells disrupting their processes such as apoptosis and reactive oxygen species production creating conditions for its growth. Historically controlling the disease in breeding involved monitoring of larvae at every stage to detect and isolate infected individuals. Preventing spores from affecting host cells and their transmission is crucial in halting the disease spread.

Studies suggest that certain proteins produced by *Nosema bombycis* may play a role in infection transmission surface wall proteins (SWPs) on the exospore which are likely to participate in host cell interactions such, as binding or signaling[5]. The exact mechanisms of their involvement remain partially understood. For instance, research has shown that certain surface wall proteins (SWPs) have the ability to attach to proteoglycans and mucin. This binding allows spores to stick to the mucin layer of the tract making it easier for the polar tube to penetrate epithelial cells during germination[5]. Endospore-associated surface wall proteins (SWPs) are most likely involved in the processes of spore germination, polar tube contact and endospore production.

Since its discovery by Louis Pasteur decades ago, *Nosema bombycis*, the microsporidian that infects the silkworm *Bombyx mori*, has served as a model organism for microsporidian research[6]. Proteomic study from *Nosema bombycis* revealed 14 putative SWPs[6]. The polar tube (PT) is attached to the host surface by the interaction of mannose binding proteins (MBPs) and polar tube protein 1 (PTP1). The polar tube can penetrate the host cell membrane and can form an invasion synapse[5]. The extruded microsporidian sporoplasm is enclosed in a protective milieu by PTP1 (and potentially PTP4) interactions with the host cell membrane at the invasion synapse. PTP4 epitopes at the tip of the polar tube attach to other host cell interacting proteins (HCIPs) or Transferrin receptor 1 (TfR1) on the surface of the host cell to start signaling pathways like clathrin-mediated endocytosis[6].

A parasitophorous vacuole forms as a result of this contact engaging the host cell actin in the final invasion step. Many of these proteins are unique to *Nosema bombycis*, while having parallels in the genomes of other microsporidia[5]. NbSWP5, NbSWP16 and NbSWP32 are located in the exospore, while NbSWP25, NbSWP30 and EOB14572 are located in the endospore, according to immunoelectron microscopy investigations[5]. Both the polar tube and the spore wall contained NbSWP7 and NbSWP9. Yang and colleagues[21,22] worked on the mature spore and sporoblast membrane structures. The spore wall's exterior and inside were both discovered to contain NbSWP1.

During endospore development, NbSWP26 was mostly expressed in the endospore and plasma membrane; however, it was only weakly expressed in the mature spores' exospore[5]. Heparin-binding motif and signal peptide are anticipated features of SWP25. Analysis using immunoelectron microscopy showed that this protein is found inside the endospore[20]. According to Yang et al[21,22], microsporidia can secrete metabolic enzymes into host cells. Hexokinase derived from microsporidia has acquired signal peptides and is released into host cells by multiple species, including i *N. bombycis* and *A. locustae*.

These proteins may have a function in controlling transcription because they have been seen to localize in the host nucleus, cytoplasm and extracellular coat of the meront. Microsporidia hexokinases phosphorylate glucose with enzymatic properties that are similar to other hexokinases, suggesting that the secretion of this enzyme is to phosphorylate host glucose, which is then taken up by the parasite cell[21,22]. Spores that are present outside the cells are prevented from extruding the polar tube and can thus avoid infecting the cells. When these spores adhere to the host cell due to other spore wall proteins, the host cell's immune system eliminates them by the process of phagocytosis. Spore wall proteins are crucial for the pathogenicity of microsporidia, aiding in their adhesion to the host organism and extruding the polar tube. Nine proteins associated with the spore wall have been identified in *Nosema bombycis*[5,6].

Material and Methods

Sequence retrieval and prediction of Tertiary proteins: The SWP12 and SWP30 sequences were obtained from UniProt database and the physio-chemical property predictions were done using a Protparam tool with the default parameter. The prediction of tertiary structure was done utilizing the I-TASSER tool. I-TASSER[21,22] is a multi-step approach that combines threading, *ab initio* modeling and iterative refinement to generate accurate 3D models of protein structures. Threading involves comparing the target protein sequence to known protein structures in a database to identify templates with significant sequence similarity. *Ab initio* modeling, on the other hand, involves constructing a 3D model of the target protein from the ground up, using fundamental physical principles. Iterative refinement involves improving the initial models through simulated annealing molecular dynamics and energy minimization steps[19].

The Galaxy Refine tools were utilized to minimize the model structure and the Ramachandran plot was produced using the RAMPAGE software to validate the model proteins. Active site prediction was carried out using the CASTP tools, which analyzed the surface of a protein structure to identify pockets and cavities likely involved in ligand binding or enzymatic activity.

This software calculates the protein's solvent-accessible surface area (SASA) and identifies pockets based on their size, shape and accessibility to solvent. Additionally, it generates a visualization of the protein structure highlighting the identified pockets.

Virtual drug screening

Molecular Docking studies: For this study, molecular docking was conducted using AutoDock Vina on 400 compounds selected based on SwissSimilarity - commercially available ZINC Drug-Like database using fumagillin as reference ligand which possesses maximum effect on microsporidians. Compounds from the ZINC database were downloaded. Initially, the molecular structures of the drugs were acquired from the PubChem website and were prepared for docking using Open Babel software[13]. SWP12 and SWP30, were prepped for docking. The docking procedure was established in AutoDock Vina which involved setting up of the search space and grid box dimensions to 60 x 60 x 60. Docking simulations were subsequently initiated, followed by evaluation of the resulting docking poses for their binding affinity.

The top docking conformations were chosen for further analysis[13,19]. PyMol (Seeliger and De Groot 2010) software was used to analyze the binding mode and interactions of the ligands with the receptor. The docking study results were utilized to assess the potential of the drug as inhibitors targeting SWP12 and SWP30 respectively.

Molecular Dynamic Simulation: Molecular dynamics (MD) simulation examines the motion of atoms in a molecule based on Newton's laws of motion[13]. The most utilized MD simulation program called GROMACS was utilized in this study. The first one was to reduce the system potential energy with the help of the cyclic alteration of atomic coordinates to optimize the protein-ligand complex in vacuum based on the steepest descent algorithm[13]. The SPC water model that abstracts water molecules as single point charges and used often as the starting model, was then used to solvate the compound in a periodic box of water. Subsequently, GaP was immersed into sodium and chloride ions to charge the system to a salt concentration of 0. 15 million[13].

To mimic the systems at 300 K and 1 bar, prevalent in biological applications, the NPT equilibration phase was conducted before the 100 ns production run in the NPT trajectory. In the trajectory analysis, there are several techniques of GROMACS that were applied including the RG, SASA, H-Bond, protein RMSD and RMSF[17]. Based on the work of Prasanth et al[12] and Gangadharappa et al[3], these analyses ensured that researchers could examine the topological and temporal characteristics of biomolecules including such parameters as the general form, flexibility and interactions with the solvent.

MMPBSA calculations: MMPBSA calculations were performed in this work using specific molecules on the SWP12 and SWP30 complexes. For these calculations, the final 50 ns of each complex's Gromacs trajectories were used[13]. First, Gromacs software was used to prepare the complicated structures for calculation. This included creating topology files and adding an explicit solvent[13]. The g_MMPBSA program was utilized to set up MMPBSA calculations and each complex underwent energy decomposition based on the last 50 ns of trajectory data. In order to assess binding affinity and comprehend the contributions of distinct energy terms to the total binding energy, the resultant energy components were examined[13]. The results of the MMPBSA were utilized to evaluate ligand binding to Human Salivary Amylase, identifying potential binding sites and interactions[9].

Results

Sequence retrieval and Tertiary structure prediction of proteins: The SWP12 and SWP30 UniProt database entries were analyzed and physicochemical properties were predicted using the Protparam tool with default parameters. Tertiary structure prediction was conducted using the I-TASSER tool, which employs a multi-step approach combining threading, *ab initio* modeling and iterative refinement to generate accurate 3D models of protein structures. Threading involves matching the target protein sequence to known protein structures in a database to identify templates with high sequence similarity. *Ab initio* modeling entails constructing a 3D model of the target protein from scratch using fundamental physical principles. Iterative refinement involves improving the initial models through simulated annealing molecular dynamics and energy minimization.

Docking result analysis: In this investigation, drug molecules were assessed for their ability to bind to SWP12 and SWP30. The binding interactions of these compounds were analyzed using molecular docking, performed using Autodock Vina software. The docking scores of the drugs against the target proteins are detailed in table 1. The table provides information on the binding affinity and the residues involved in hydrogen-forming and hydrophobic interactions for two protein compounds, SWP12 and SWP30, with the target protein DRG1. For SWP12, the binding affinity is -7.1 kcal/mol. The interactions occur with the following residues: ARG14, LYS7, ILE8, SER13, LYS18, GLU180, GLU183 and SER179. These interactions involve both hydrogen bonding and hydrophobic interactions. On the other hand, SWP30 exhibits a higher binding affinity of -8.8 kcal/mol. The residues involved in the interactions involving hydrogen bonding and hydrophobic interactions with DRG1 include GLU32, VAL62, ARG58, VAL11, LEU12, PRO21, TYR28 and HIS25.

Molecular Dynamic Simulation: Based on the docking results, SWP12 and SWP30 proteins were chosen for a molecular dynamics simulation study. The simulation was conducted on SWP12 and SWP30 both in their unbound states and in complex with ligands to investigate the dynamic behavior of these target proteins: (i) SWP12 Protein alone [SWP12-APO], (ii) SWP30 Protein alone [SWP30-APO], (iii) SWP12 Protein bound to LIG [SWP12-LIG], (iv) SWP30 Protein bound to LIG [SWP30-LIG].

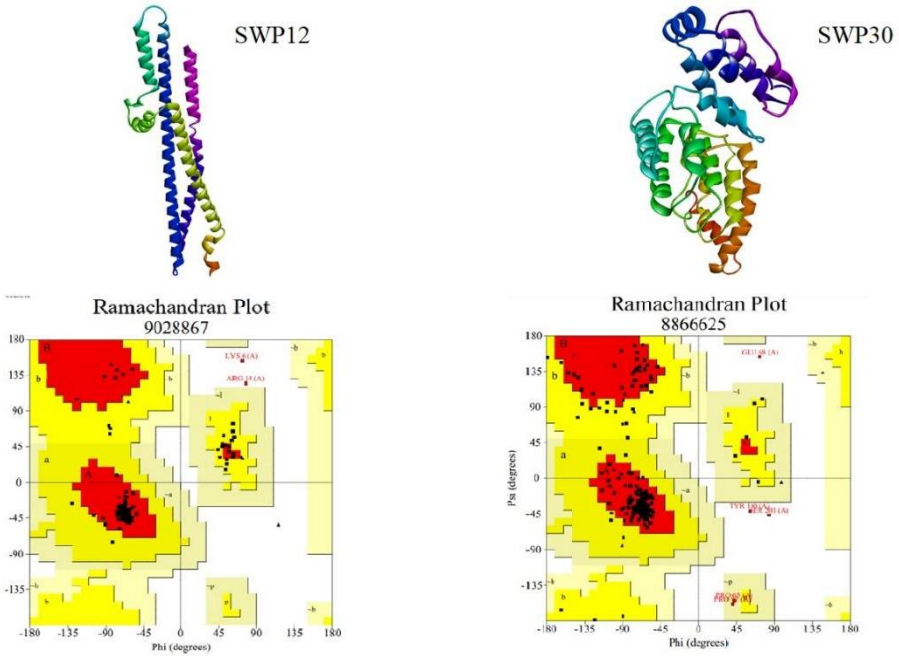

Figure 1: The 3D structure of SWP12 and SWP30 and the validation of the modeled protein using Ramachandran plot.

Table 1
Docking score and the nature of drug interaction against SWP12 and SWP30

Protein	Compound Name	Binding Affinity kcal/mol	Hydrogen-forming and hydrophobic interaction
SWP12	DRG1	-7.1	ARG14, LYS7, ILE8, SER13, LYS18, GLU180, GLU183, SER179
SWP30	DRG1	-8. 8	GLU32, VAL62, ARG58, VAL11, LEU12, PRO21, TYR28, HIS25

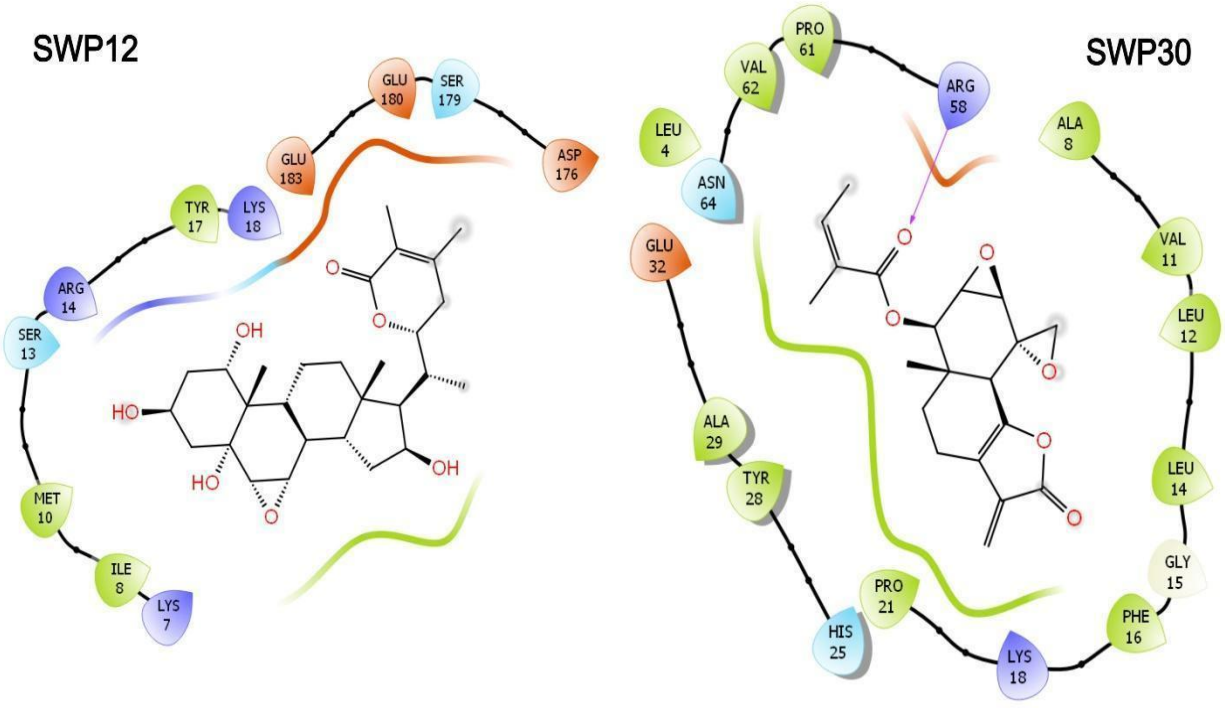

Figure 2: The docking 2D images of SWP12 and SWP30.

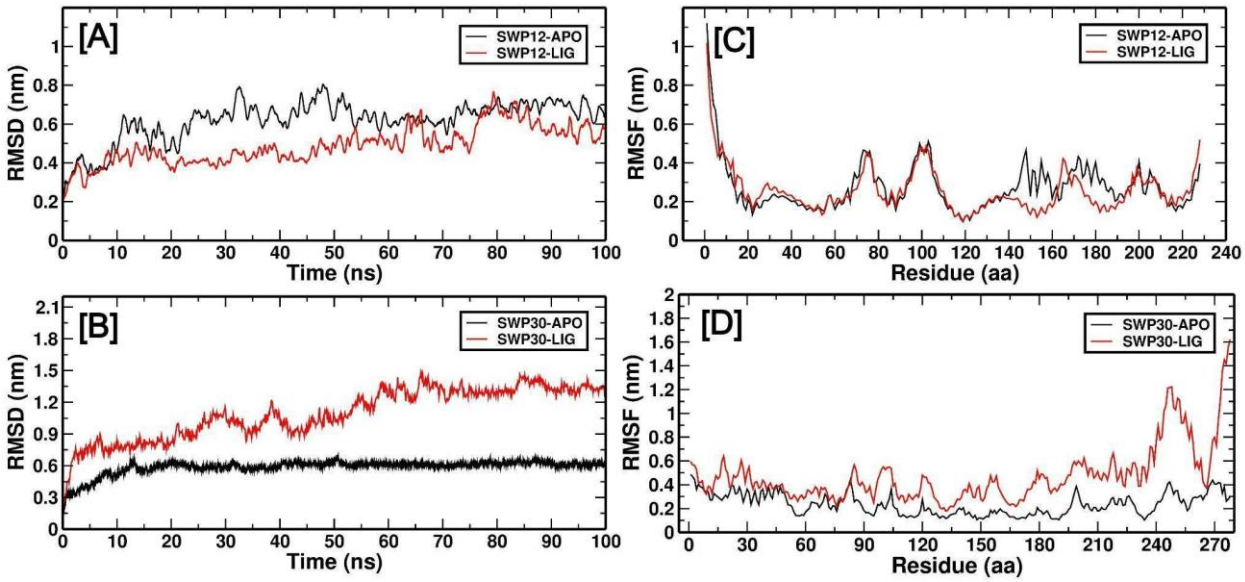

Figure 3: RMSD and RMSF graph representing MDS for 100 ns of SWP12 and SWP30.

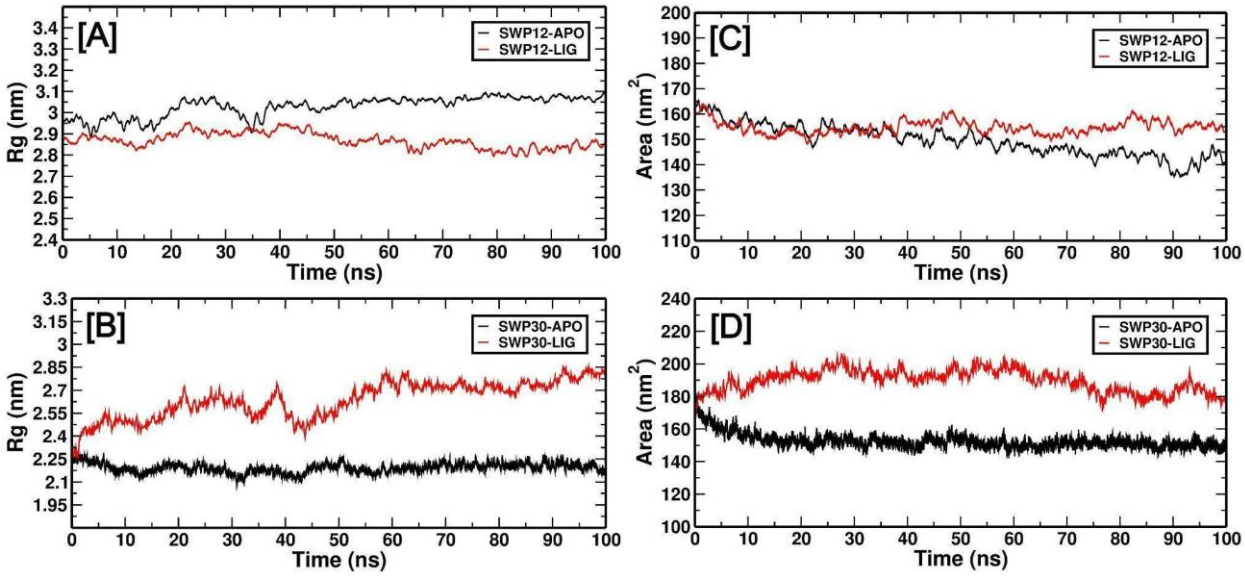

Figure 4: Rg and SASA graph representing MDS for 100 ns of SWP12 and SWP30.

In the SWP12-APO and SWP12-LIG complexes, the average of the RMSDs calculated from 0 to 100 ns were 0. 59 +/- 0. 12 nm and 0. 62 +/- 0. 13 nm respectively. Looking at the overlay of the unbound protein with the absolutely bound protein, it was clear that there were no significant differences in the RMSD analysis (Figures 3). The average RMSDs for the complexes of SWP30-APO and SWP30-LIG are 0. 61 +/- 0. 05 nm and 1. 42 +/- 0. To sum up, at 0 – 100 ns, both of the interface residues approached to be located at 7 Å and 22 nm respectively, away from the unbound protein (Figures 3). Such results suggest that while the compound complexes did not change much, both of the complexes were stable throughout the simulation. In the RMSF analysis based on the results of the 100 ns simulation, any significant structural changes were not noted. Analysis identifies the amino acids that vibrate higher, that can destabilize this protein with or without ligands. The calculated and compared measure chosen for this particular analysis was the radius of gyration, regarding the compactness and form folding over time of the structure. Throughout the simulation, SWP12-APO and SWP12-LIG both had comparable Rg values: 3. 15 +/- 0. 03 nm and 2. 94 +/- 0. The performance of the proposed codes increased on an average from 0 to 100 ns, being 14 nm (Figure 4). On the other hand, in the case of SWP30, the Rg patterns were conspicuously different. In the same simulation time, two basic values of SWP30-APO and SWP30-LIG are 2. 25 +/- 0. 13 nm and 2. 55 +/- 0. and nonsignificant difference was observed between the two groups in needed airspace vertical clearance with 15 ± 4 for LAP<|reserved_special_token_263|> and 14 ± 5 for MAP, respectively (Figure 4).

Analyses were also performed with respect to the solvent accessible surface area (SASA) to determine the compactness of the core. For SWP12, the SASA averages of

the SWP12-APO and SWP12-LIG structures are 152. 07 +/- 3. 60 nm and 154. 13 +/- 5. is 0 to 20 nm and 0 to 100 ns for E and 20 nm and 100 ns for palladium respectively. Meanwhile, the average SASA values for simulation period of three weeks for SWP30 were 159. 01 +/- 4. For the SWP30-APO complex, it is 30 nm while that of the SWP30 solution it is 178. 11 +/- 5. 20 nm for the SWP30-LIG complex. Based on these findings, it can be postulated that the protein's structure did not change much throughout the simulation.

MM – PBSA: Of the two form lists, one was employed for the identification of the binding energy of SWP12-LIG and the other for the identification of SWP30-LIG relative to the strength of binding inside the protein. Table 2 lists the binding free energy estimates of the inhibitors toward SWP12-LIG and SWP30-LIG based on the MM-PBSA analysis. Thus, we assessed residue-by-residue contributions to the interaction energy at every step of a stable simulation period.

Thermoneutral energy of – 38 kJ/mol and electrostatic energy of – 14. 389 +/- 13. -2 kJ/mol measured standard enthalpies of sublimation of 696 kJ/mol. 090 +/- 26. Enthalpy of formation is 391 kJ/mol and binding energy is of -108. 978 +/- 40. As stated in the results, for SWP12-LIG, the values are 651 kJ/mol. On the other hand, SWP30-LIG has the binding energy of -29 Kcal/mol. 872 +/- 61. 316 kJ/mol and a polar solvation energy of 5. 146 +/- 59. 240 kJ/mol and an electrostatic energy of - 0. 544 +/- 6. The bond dissociation energy is 902 kJ/mol and the van der Walls energy is -29 kJ/mol. 927 +/- 33. 474 kJ/mol. It can be concluded from the obtained results that there are differences in the van der Waals, electrostatic, polar solvation and binding energies of the two compounds. These differences are due to difference in the different chemical characteristics of the different chemicals. Thus, further analysis is needed.

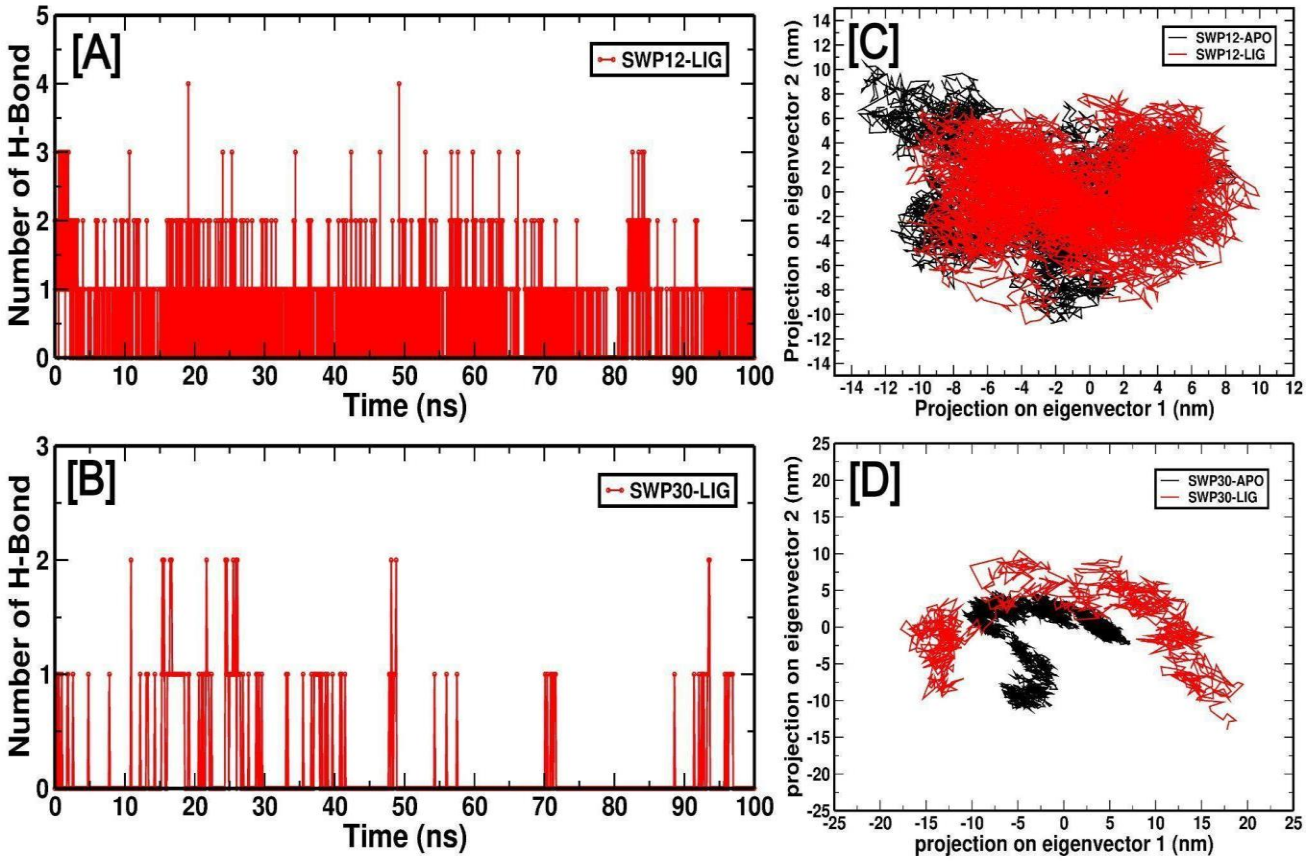

Figure 5: Comparison of Hydrogen bond and PCA of SWP12 and SWP30

Table 2
Van der Waals energy, electrostatic energy, polar solvation energy and binding energy of the protein-ligand complexes

System	van der Waal energy	Electrostatic energy	Polar solvation energy	Binding energy
SWP12-LIG	-145.012 +/- 50.038 kJ/mol	-14.389 +/- 13.696 kJ/mol	66.090 +/- 26.391 kJ/mol	-108.978 +/- 40.651 kJ/mol
SWP30-LIG	-29.927 +/- 33.474 kJ/mol	-0.544 +/- 6.902 kJ/mol	5.146 +/- 59.234 kJ/mol	-29.872 +/- 61.316 kJ/mol

Discussion

The silk industry had been facing a severe problem of huge economical losses for centuries because of pebrine infection caused by the microsporidian *Nosema bombycis*. That is the explanation of the cross-colonial transmission both horizontally and vertically; making the rate of infection significantly fast[7]. Upon entry into the host cell, the parasite suppresses apoptosis and the formation of reactive oxygen species ensuring the requirements for replication are met. To be able to quantify the controllability of disease dissemination, actions against spore dispersal and the minimization of host cell injury must be accomplished. *Nosema bombycis* has been shown to synthesize numerous proteins associated with the dissemination of infections but the processes through which these proteins operate are not well understood.

In this study, the genetic information of the structural proteins of the spore wall of *N. bombycis* including SWP9, SWP12, SWP26, SWP30 and SWP32 are critical. These proteins are involved in attaching to the spore wall and germinating besides preceding the organization of polar tube. SWP12 is one of the major surface proteins of the *N. bombycis* and this chitin-binding spore wall protein is necessary for spore wall synthesis. Located primarily on the outer surface of the *N. bombycis* cytoskeleton and within the spore coat, it plays a role in microsporidial spores' protection and possibly in signal transfer. As an endosporal protein related to sporulation and the yield of cellular spores, SWP30 is located inside the spore coat[10]. This protein is synthesized during sporogony while its antibody rejects deproteinated chitin spore coatings (DSCS).

Research has shown that when a mature spore is treated or coated with an anti-SWP, then the subsequent formation of the polar tube as well as the ingestion of the spore by the host cell is also reduced[22]. This finding opens the notion of controlling or even reversing the progression of the disease by preventing SWP proteins from acting. Therefore, the aim has been directed towards identification of the pharmacological candidates that may suite the protein pockets of SWP12 and SWP30 and thereby inhibit the process of extrusion of the terminal polar tube in the phagocytosis of the host cell.

For this study, The SWP12 and SWP30 UniProt database entries were analyzed and physicochemical properties were predicted using the Protparam tool with default parameters. The tertiary structures of the proteins were modeled using I-TASSER[4,14,21]. The model with the highest confidence score was chosen and subsequently validated. The low-resolution models predicted by this server were further refined by ModRefiner algorithm to obtain high resolution models. The Galaxy Refine tools were utilized to minimize the model structure and a Ramachandran plot was generated using the RAMPAGE tool to validate the model proteins. The prediction of active sites was performed using CASTP tools which analyze the surface of a protein structure to identify pockets and cavities likely to be involved in ligand binding or enzymatic activity. This software calculates the solvent-accessible surface area (SASA) of the protein and identifies pockets based on their size, shape and accessibility to solvent. Additionally, it generates a visualization of the protein structure highlighting the identified pockets. Molecular docking was conducted utilizing AutoDock Vina[18] on 400 compounds selected based on SwissSimilarity - commercially available ZINC Drug-Like database using Fumagillin as reference ligand which possesses a maximum effect on microsporidians. From the ZINC database, these compounds were downloaded.

Docking runs were then initiated using the methodology mentioned earlier and the resulting docking conformations were evaluated for their binding affinity for selecting the top poses[13,19]. The results of the docking study were used to evaluate the potential of the drugs as inhibitors of the SWP12 and SWP30 respectively. From the analysis performed, drug molecules were assessed for their capacity to bind to SWP12 and SWP30. SWP12 and SWP30, with the target protein DRG1. For SWP12, the binding affinity is -7.1 kcal/mol. The interactions occur with the following residues: ARG14, LYS7, ILE8, SER13, LYS18, GLU180, GLU183 and SER179. These interactions involve both hydrogen bonding and hydrophobic interactions.

On the other hand, SWP30 exhibits a higher binding affinity of -8.8 kcal/mol. The residues involved in the hydrogen-forming and hydrophobic interactions with DRG1 include GLU32, VAL62, ARG58, VAL11, LUE12, PRO21, TYR28 and HIS25 (Table 1). This procedure showed binding affinity of proteins which can be considered for further analysis. In the first step, applying steepest descent approach, the complex formed between the protein and ligand was minimized in vacuum[13]. This was then accompanied by solvation in a periodic water box according to SPC water model. Subsequently, the complex was given time for equilibrating at a definite amount of salt concentration which in this case was 0. 15 M while being maintained at a constant pressure and a constant temperature of 1015 NPT.

Therefore, to study some of the structural and dynamic characteristics of the simulated system like the shape, flexibility and the interactions with the solvent GROMACS software, a molecular production run of 100 ns in the NPT ensemble was conducted. Facilities associated with these included RG, SASA, RMSD, RMSF, H-Bond. In order to better understand the dynamic behavior of the two targeted proteins, SWP12 and SWP30 in their apo-form conformation and in the protein-ligand complex conformations have been selected. Thus, there was no effect on the average root mean square deviation (RMSD) 0. 59 +/- 0. 0.7 nm for SWP12-APO and 0. 62 +/- 0. 2 Å for the complex of SWP12-LIG during 0-100 ns simulations (Figure 3).

Nevertheless, in the cases of the SWP30-APO and SWP30-LIG proteins, the average RMSDs from 0 to 100 ns were equal to 0. 61 +/- 0. 05 nm and 1. 42 +/- 0. 22 nm, respectively while the distance between the other residues of the protein is around 14 nm, this information shows a relative stability of the compound complexes in the course of the simulation from the unbound protein in general (Figure 3). RMSF values calculated for the range of 0–100 ns of simulation did not reveal any significant changes in a structural level. From the radius of gyration (Rg) study of SWP12 in this project (Fig. 4), it could be noted that Rg values for both SWP12-APO and SWP12-LIG remained constant throughout the simulation and those average values fell around 3. 15 +/- 0. 03 nm and 2. 94 +/- 0. From 0 to 100 ns, both fall and rise time are checked to be at 7 ns and 14 nm individually.

On the other hand, over the course of the simulation, Rg patterns of SWP30-APO and SWP30-LIG changed, their averages being 2. 25 +/- 0. 13 nm and 2. 55 +/- 0. 14 nm respectively. In contrast, for SWP30-APO and SWP30-LIG, the solvent-accessible surface area (SASA) values were 159.01 +/- 4.30 nm and 178.11 +/- 5.20 nm, respectively, showing no change in protein structural levels throughout the simulation. The values for SWP12-APO and SWP12-LIG were 152.07 +/- 3.60 nm and 154.13 +/- 5.20 nm, respectively, over 0 to 100 ns. The 50 ns were employed for energy decomposition calculations of each complex in the MMPBSA calculations which were set up with the software g_MMPBSA[13]. Subsequent energy values were applied to analyze the energy terms' participation towards the total binding energy and binding affinity[13].

A thorough understanding on the interaction and the evaluation of ligand binding to the Human Salivary Amylase enzyme along with identification of putative binding sites along with interaction were facilitated by this analysis[9]. The binding strength was computed concerning the inhibitors by implementing the MM-PBSA method and entailing interaction energy at the residue level to analyze the binding affinity of both SWP12-LIG and SWP30-LIG. The van der Waals energy and the electrostatic energy for SWP12-LIG are given in table 2 along with the polar solvation energy and the binding energy. From the van der Waals plot, the van der Waals energy was estimated to be -145. 012 +/- 50.

Computed at 038 kJ/mol, the electrostatic energy was -14. 389 +/- 13. 696 kJ/mole and the binding energy was -108. 978 +/- 40. 651 kJ/mol. Comparably, SWP30-LIG showed -29. 927 +/- 33. 474 kJ/mol for van der Waals energy, -0. 544 +/- 6. The raw energy data for a diatomic molecule for IE and EA is IE = 902 kJ/mol for electrostatic energy; 5. 146 +/- 59. Polar solvation energy is - 234 kJ/mol and dipole moment is - 29 D. 872 +/- 61. The binding energy was 316 kJ/mol as found in the table 2.

The results represented here reveal binding and partial molar quantity values, together with solvation and other energies, for the purpose of comparison at the basis of the different architectures and characteristics of the compounds in question. This means that additional work has to be done in order to pinpoint more concrete conclusions, based on the presented data. These outcomes suggest that SWP12 and SWP30 have strong binding affinity with DRG1 which has mainly hydrophobic and hydrogen forming contact.

Understanding those specific interactions enables one to comprehend molecular processes and possible applications of these protein compounds in various biological processes or cure methods. Low standard deviations in Rg indicate that off target motion did not change the size of the protein complexes considerably over the trajectory time points suggesting structural integrity over the course of simulation.

Conclusion

The objective of the experiment was to identify compounds that bind to the microsporidial spore wall proteins SWP12 and SWP30 through the *in silico* approach. Some validated compounds may act as therapeutic molecules against *N.bombycis* biochemistry to reduce its recognition of the host's immune system, attachment to spores and infectivity of *B. mori* to control Pebrine illness. In the context of this study, candidate therapeutic agents against SWP12 and SWP30 in pathogenic cells were sought and they included energy minimization, molecular docking, ligand-based virtual screening, protein structure prediction and molecular dynamics simulation.

Through the virtual screening and docking experiments, compounds named ZINC000067910920 and ZINC000035458200 were predicted to be new potent drug-like molecules. MD simulations provide insights on the way the ligand molecules engage the interaction with SWP12 and SWP30 proteins. The UniProt IDs are SWP12_NOSB1 and SWP30_NOSB1, the protein sequences of SWP12 and SWP30 were downloaded in FASTA format from the UniProt Database. Due to their large sizes, I-TASSER was employed to predict the two proteins' structures.

The NbSWP12-ZINC000067910920 and SWP30-ZINC000035458200 complexes were subjected to molecular dynamics simulations using the Schrödinger DESMOND package version 2017:3[1], The Cluspro2. To predict the conformation of these interactions 0 server was used and to check the predicted conformation of the interaction with the least energy, DIMPLOT was employed. Further research could analyze other proteins belonging to the family of the spore wall proteins that actively take part in the process of infection.

Acknowledgement

Mr. Vivek Chandramohan, SIT, Tumakuru is acknowledged for providing the MM-GBSA results using Accelrys Discovery studio and critical discussion associated with molecular dynamics simulations.

References

1. Bowers K.J. et al, Scalable algorithms for molecular dynamics simulations on commodity clusters, Proceedings of the 2006 ACM/IEEE Conference on Supercomputing, SC'06, https://doi.org/10.1145/1188455.1188544 **(2006)**

2. Bukhari T., Pevsner R. and Herren J.K., Microsporidia: a promising vector control tool for residual malaria transmission, *Front. Trop. Dis.*, **3**, 957109, doi: 10.3389/fitd.2022.957109 **(2022)**

3. Gangadharappa, Somalapura Bhavya, Sharath Rajashekarappa, Revanasiddappa Prasanna D., Chandramohan Vivek, Balasubramaniam Meenakshisundaram and Vardhineni Teja Priya, Structural Insights of Metallo-Beta-Lactamase Revealed an Effective Way of Inhibition of Enzyme by Natural Inhibitors, *Journal of Biomolecular Structure and Dynamics*, **38(13)**, 3757–71, https://doi.org/10.1080/07391102.2019.1667265 **(2020)**

4. Gasteiger E., Hoogland C., Gattiker A., Wilkins M.R., Appel R.D. and Bairoch A., Protein identification and analysis tools on the ExPASy server, In The proteomics protocols handbook, Humana, 571-607 **(2005)**

5. Han B. and Weiss L.M., Microsporidia: Obligate Intracellular Pathogens Within the Fungal Kingdom, *Microbiol Spectr*., **5(2)**, doi: 10.1128/microbiolspec.FUNK-0018-2016 **(2017)**

6. Han Bing, Takvorian Peter M. and Weiss Louis M., Invasion of Host Cells by Microsporidia, *Frontiers in Microbiology*, **11**, https://doi.org/10.3389/fmicb.2020.00172 **(2020)**

7. James, Rosalind R. and Zengzhi Li, From Silkworms to Bees: Diseases of Beneficial Insects, In Insect Pathology, Second Edition, Elsevier, 425–59, https://doi.org/10.1016/B978-0-12-384984-7.00012-9 **(2012)**

8. Karunakar P., In silico modelling and virtual screening for identification of inhibitors for spore wall protein-5 in Nosema bombycis, *J Biomol Struct Dyn*., **40(4)**, 1748-1763, doi: 10.1080/07391102.2020.1832579 **(2022)**

9. Kumari Rashmi, Kumar Rajendra and Lynn Andrew, G-Mmpbsa -A GROMACS Tool for High-Throughput MM-PBSA Calculations, *Journal of Chemical Information and Modeling*, **54(7)**, 1951–62, https://doi.org/10.1021/ci500020m **(2014)**

10. Li Y., Wu Z., Pan G., He W., Zhang R., Hu J. and Zhou Z., Identification of a novel spore wall protein (SWP26) from microsporidia Nosema bombycis, *Int J Parasitol*., **39(4)**, 391-8, doi: 10.1016/j.ijpara.2008.08.011 **(2009)**

11. Prior Chris, Insect Pathology, Tanada Y. and Kaya H., San Diego, USA, Academic Press Inc., **(1992)**

12. Prasanth D. et al, In Silico Identification of Potential Inhibitors from Cinnamon against Main Protease and Spike Glycoprotein of SARS CoV-2, *Journal of Biomolecular Structure and Dynamics*, **39(13)**, 4618–32, https://doi.org/10.1080/07391102.2020.1779129 **(2021)**

13. Ravikumar Y., Koonyosying P., Srichairatanakool S., Ponpandian L.N., Kumaravelu J. and Srichairatanakool S., In Silico Molecular Docking and Dynamics Simulation Analysis of Potential Histone Lysine Methyl Transferase Inhibitors for Managing β-Thalassemia, *Molecules*, **28(21)**, 7266, doi: 10.3390/molecules28217266 **(2023)**

14. Roy A., Kucukural A. and Zhang Y., I-TASSER: a unified platform for automated protein structure and function prediction, *Nature Protocols*, **5**, 725-738 **(2010)**

15. Seeliger Daniel and De Groot Bert L., Ligand Docking and Binding Site Analysis with PyMOL and Autodock/Vina, *Journal of Computer-Aided Molecular Design*, **24(5)**, 417–22, https://doi.org/10.1007/s10822-010-9352-6 **(2010)**

16. Sharma P., Joshi T., Mathpal S., Chandra S. and Tamta S., In silico identification of antidiabetic target for phytochemicals of A. marmelos and mechanistic insights by molecular dynamics simulations, *J Biomol Struct Dyn*., **40(21)**, 10543-10560, doi: 10.1080/07391102.2021.1944910 **(2022)**

17. Su J., Sun T., Wang Y. and Shen Y., Conformational Dynamics of Glucagon-like Peptide-2 with Different Electric Field, *Polymers (Basel)*, **14(13)**, 2722, doi: 10.3390/polym14132722 **(2022)**

18. Trott Oleg and Arthur Olson J., AutoDock Vina: Improving the Speed and Accuracy of Docking with a New Scoring Function, Efficient Optimization and Multithreading, *Journal of Computational Chemistry*, **31(2)**, https://doi.org/10.1002/jcc.21334 **(2009)**

19. Tung C.S., Walsh D.A. and Trewhella J., A structural model of the catalytic subunit-regulatory subunit dimeric complex of the cAMP-dependent protein kinase, *J Biol Chem*., **277(14)**, 12423-31, doi: 10.1074/jbc.M110298200 **(2002)**

20. Wu Z., Li Y., Pan G., Zhou Z. and Xiang Z., SWP25, a novel protein associated with the Nosema bombycis endospore, *J Eukaryot Microbiol*., **56(2)**, 113-8, doi: 10.1111/j.1550-7408.2008.00375.x **(2009)**

21. Yang J., Yan R., Roy A., Xu D., Poisson J. and Zhang Y., The I-TASSER Suite: Protein structure and function prediction, *Nature Methods*, **12**, 7-8 **(2015)**

22. Yang Donglin et al, Interaction between SWP9 and Polar Tube Proteins of the Microsporidian Nosema Bombycis and Function of SWP9 as a Scaffolding Protein Contribute to Polar Tube Tethering to the Spore Wall, *Infection and Immunity*, **85(3)**, https://doi.org/10.1128/IAI.00872-16 **(2017)**

23. Zhangwuke Fu, Mingqian Li, Han Liu, Shunfeng Cai, Nana Man and Xingmeng Lu, Nosema Bombycis (Microsporidia) Suppresses Apoptosis in BmN Cells (Bombyx Mori), *Acta Biochimica et Biophysica Sinica*, **47(9)**, 696–702, https://doi.org/10.1093/abbs/gmv062 **(2015)**.

(Received 16th October 2024, accepted 18th December 2024)